Soft Matter

Actin and microtubule crosslinkers tune mobility and control co-localization in a composite cytoskeletal network

Journal:	*Soft Matter*
Manuscript ID	SM-ART-12-2019-002400.R1
Article Type:	Paper
Date Submitted by the Author:	09-Feb-2020
Complete List of Authors:	Farhadi, Leila; University of Massachusetts Amherst, Department of Physics Ricketts, Shea; University of San Diego, Rust, Michael; University of Chicago Das, Moumita; Rochester Institute of Technology, Robertson-Anderson, Rae; University of San Diego, Physics and Biophysics Ross, Jennifer; Syracuse University, Physics; University of Massachusetts Amherst, Department of Physics

Actin and microtubule crosslinkers tune mobility and control co-localization in a composite cytoskeletal network

Leila Farhadi[a], Shea N. Ricketts[b], Michael J. Rust[c], Moumita Das[d], Rae M. Robertson-Anderson[b], and Jennifer L. Ross*[a]

[a]Department of Physics, University of Massachusetts, Amherst, 666 N. Pleasant St., Amherst, MA 01003

[b]Department of Physics and Biophysics, University of San Diego, 5998 Alcala Park, San Diego, CA 92110

[c]Department of Molecular Genetics and Cell Biology, University of Chicago, University of Chicago, 900 E 57th St, Chicago, IL 60637

[d]School of Physics and Astronomy, Rochester Institute of Technology, 84 Lomb Memorial Drive, Rochester, NY 14623

*rossj@physics.umass.edu

Abstract

Actin and microtubule filaments, with their auxiliary proteins, enable the cytoskeleton to carry out vital processes in the cell by tuning the organizational and mechanical properties of the network. Despite their critical importance and interactions in cells, we are only beginning to uncover information about the composite network. The challenge is due to the high complexity of combining actin, microtubules, and their hundreds of known associated proteins. Here, we use fluorescence microscopy, fluctuation, and cross-correlation analysis to examine the role of actin and microtubules in the presence of an antiparallel microtubule crosslinker, MAP65, and a generic, strong actin crosslinker, biotin-NeutrAvidin. For a fixed ratio of actin and microtubule filaments, we vary the amount of each crosslinker and measure the organization and fluctuations of the filaments. We find that the microtubule crosslinker plays the principle role in the organization of the system, while, actin crosslinking dictates the mobility of the filaments. We have previously demonstrated that the fluctuations of filaments are related to the mechanics, implying that actin crosslinking controls the mechanical properties of the network, independent of the microtubule-driven re-organization.

Introduction

The cytoskeleton is composed of interacting biopolymer filaments that regulate the spatial organization and mechanical properties of the cell. Actin filaments are composed of two protofilaments made from actin monomers, helically twisted with a diameter of 7 nm and a persistence length of 10 μm [1–3]. Actin filaments and their actin binding proteins (ABPs) govern cell migration, contraction, and cell signaling [4]. Microtubules are composed of tubulin protein dimers that form a lattice of 13 protofilaments that roll into a tube to create a hollow cylinder structure with an outer diameter of 25 nm and a persistence length of 1mm [5–7]. Microtubules, the microtubule associated proteins (MAPs), and enzymes control intracellular transport, mitotic spindle formation, and cellular organization. The distinct structures and physical properties of these cytoskeletal subunits enable the cell to maintain its integrity during cell growth, differentiation, division, and motility [2].

Characterizing the dynamics and mechanics of composite cytoskeletal networks is important for both biological and synthetic applications. On the biological front, intracellular experimental are complex and uncontrolled. Clean, reproducible *in vitro* experiments enable the elucidation of fundamental principles of cytoskeletal organization and mechanics [8–10]. From a synthetic materials view, cellular composite networks inspire the design and fabrication of smart synthetic and biomimetic materials with tunable mechanical properties [11,12].

Most of the studies of *in vitro* reconstitution of cytoskeletal filaments have been conducted in a network of either actin or microtubule filaments. The mechanics and dynamics of co-entangled and crosslinked actin networks have been characterized in the presence of various crosslinkers with different structures and strength, such as alpha-actinin, fascin, palladin, arp 2/3, arg, filaminA, and biotin-NeutrAvidin [13–22]. It has been shown that actin crosslinkers can increase elasticity and stiffness of the network and lead to the formation of actin bundles [1,18,19,23,24]. Microtubule network organization and mechanics have also been explored in the presence of MAP65, Ase1, PRC1, biotin-NeutrAvidin, and active crosslinkers like various types of kinesin motors with different movement direction and speed [13,25–39]. The viscoelasticity measurements showed that entangled microtubule networks are soft elastic solids while intermediate amounts of crosslinkers make a stiffer gel of filaments [40].

Despite their biological relevance, few studies have explored composite networks of actin and microtubule filaments. These studies have shown that the interactions between these filaments lead to unexpected emergent properties [14,41–53]. For example, we have previously shown that actin filaments, rather than microtubules, govern the microscale elasticity and mobility of actin-microtubule composite networks comprised of equal molar ratios of actin monomers and tubulin dimers [13,14,49]. We showed that this effect was due to the smaller mesh size of the network of actin filaments compared to that of the microtubules in the composite[14]. Here, we sought to examine networks with more comparable mesh sizes from similar total filament lengths. Using a fixed ratio of actin to microtubules, we independently varied the actin and microtubule crosslinkers. We used biotin-NeutrAvidin to permanently crosslink actin filaments, and MAP65 to transiently crosslink microtubules. We found that actin crosslinkers tune the mobility of the composite network: actin becomes less mobile, while microtubules become more mobile. Microtubule crosslinkers, on the other hand, control the co-localization of actin and microtubule filaments in the composite network.

Materials and Methods

Rabbit skeletal actin, biotinylated actin, and rhodamine-labeled actin were purchased from Cytoskeleton (AKL99, AB07, AR05) and resuspended at 2 mg/ml, 1 mg/ml, and 1.5 mg/ml, respectively, in Ca Buffer G (2 mM Tris pH 8.0, 0.2 mM ATP, 0.5 mM DTT, 0.1 mM $CaCl_2$) and stored at -80ºC. Lyophilized porcine brain tubulin, biotinylated tubulin, fluorescent HiLyte 488-labeled tubulin, and fluorescent HiLyte 647 tubulin were purchased from Cytoskeleton (T240, T33P, TL488M, TL670M). Porcine tubulin and biotinylated tubulin were resuspended to 5 mg/ml in PEM-100 [100 mM PIPES (pH 6.8), 2 mM $MgCl_2$, 2 mM EGTA] and stored at - 80ºC. HiLyte 488 or 647-labeled tubulin was resuspended to 5 mg/ml using a ratio of 1:10 fluorescent labeled tubulin:unlabeled-tubulin in PEM-100 and stored at -80ºC.

Two different types of crosslinkers were used in composite networks of actin and microtubules. To crosslink actin filaments, biotin-NeutrAvidin crosslinker complexes were prepared according to previously published protocols [13,14]. To crosslink microtubule filaments, GFP labeled and unlabeled MAP65-1 was used that was expressed and purified from bacteria as previously described [36,54,55].

Composite networks were made by mixing tubulin, G-actin, and crosslinkers in PEM-100 solution. For visualization, biotinylated, rhodamine labeled actin filaments were pre-polymerized in PEM-100 and 2 mM ATP by incubation for 1 hour in room temperature. To visualize microtubules, all filaments were labeled with HiLyte 488 or HiLyte 647. Pre-polymerized, rhodamine-labeled actin filaments were prepared at 5 μM with 1:1 rhodamine labeled actin:unlabeled actin monomer ratio and 0, 0.04, 0.08, or 0.16 biotin-actin:total actin monomer ratio. A mixture of unlabeled and HiLyte 488-labeled or HiLyte 647-labeled tubulin (with 3:100 labeled:unlabeled tubulin, 9.1 μM total), unlabeled actin monomer (1.43 μM final concentration) and pre-polymerized rhodamine labeled actin filaments (1.43 μM final concentration) were added to the PEM-100 buffer with 1 mM ATP, 1 mM GTP and 5 μM Taxol. Oxygen scavenging agents (4.5 mg/ml glucose, 4.3 mg/ml glucose oxidase, 0.7 mg/ml catalase, and 0.5% β-

mercaptoethanol,) were added to the solution to inhibit photobleaching. Additionally, 0.025% Tween was included to block the chamber surface from protein binding. The mixture was pipetted into a ~10 μL sample chamber made of a glass slide and cover slip attached via permanent double stick tape (3M). The ends were sealed by epoxy and the sample chamber incubated at 37°C for 30 minutes to form the composite network.

At the concentrations of actin and tubulin proteins used, 1.4 μM and 9.1 μM, respectively, the mesh size of actin and microtubule networks are estimated as $\xi_A = 0.3/c_A^{1/2} = 1.22$ μm and $\xi_M = 0.89/c_T^{1/2} = 0.89$ μm, respectively, where c_A and c_T are the actin and tubulin concentrations in units of mg/ml [56–58]. We can estimate the total polymer length in our 10 µl experimental chamber from the concentrations and known geometries of the filaments. For actin, we estimate that there are 27 actin monomers in a 72 nm length of actin filament. Given the concentration of 1.4 μM, we estimate the total polymer length, when all actin monomers go into polymer form to be 2.4 x 10^4 m. For microtubules, we estimate that there are 13 dimers for a 12 nm length of filament. Given the concentration of 9.1 μM, we estimate the total polymer length, when all tubulin dimers are polymerized to be 5 x 10^4 m. These two total polymer lengths are the same order of magnitude, so we conclude that the total polymer length present is approximately one-to-one. In all of the presented data, the total molar concentration of actin and tubulin were fixed while the crosslinker concentrations varied. NeutrAvidin:actin molar ratios of R = 0, 0.02, 0.04, and 0.08 were examined for actin crosslinking. For microtubules, three different percentages of MAP65, 0%, 3%, and 10%, were tested. The % represents the percentage of tubulin dimers that are bound to MAP65 crosslinkers. The percent bound was determined from the known equilibrium dissociation constant, as previously described [25]. We specifically use different nomenclature for the amount of actin and microtubule crosslinkers because this is the nomenclature from prior literature [13,14,25,55] and to make it less confusing about which filament crosslinker we are referring.

We use a Nikon Ti-E inverted microscope with a 60x water immersion objective (NA = 1.38) with scientific-CMOS camera (Zyla). The pixel size was 108 nm/pixel and the diffraction limit was around 300 nm, roughly corresponding to 3 pixels. The microscope can record 2048x2048 images in green and red channels alternatively to visualize fluorescent HiLyte 488-labeled microtubules and rhodamine labeled actin filaments. For each experiment at a specified actin and microtubule crosslinker ratio, 5-10 time series were recorded that were 1 to 1.5 minutes each. The exposure time was 60 ms and 100 ms for the green and red channels, respectively.

To quantify the mobility of the composite network, FIJI/ImageJ was used to analyze each channel separately, as described previously [13,14]. Briefly, the standard deviation and average of the intensity of an image series were measured. Then the mean values of each channel were measured and used to calculate $<\delta>/<I>$ where $<\delta>$ is the average standard deviation of intensity measurement over the entire time series and $<I>$ is the average intensity mean over time series. These measurements were calculated for the actin and microtubule fluorescence channels separately. The value of this ratio determined the mobility of actin and microtubule filaments within each composite network.

To characterize the co-localization of microtubules and actin filaments, we calculated the cross correlation between microtubule and actin fluorescence channels for the same location and time. For each image of the same region in the chamber recorded from the actin channel and the microtubule channel, we can calculate the local normalized cross-correlation value for a region of n pixels. The definition of normalized cross correlation is:

$$< I_a * I_m >= \frac{1}{n} \sum_{x,y} \frac{(I_a(x,y) - \mu_a)(I_m(x,y) - \mu_m)}{\sigma_a \sigma_m} \qquad \text{Eq 1}$$

where $I_a(x,y)$ and $I_m(x,y)$ are the intensity values for the x and y coordinates of the selected, corresponding regions of interest over which the normalized cross correlation is calculated. The parameters μ_a and μ_m

are the mean intensity values, and σ_a and σ_m are the standard deviations of intensities for the same region. This definition of normalized cross correlation returned values between -1 and +1, where +1 values denote high correlation between the actin and microtubule images and were depicted in white, -1 values indicated anti-correlation between the actin and microtubule images and were depicted in black; intermediate scaled linearly in grey.

We can use this definition of the normalized cross-correlation function to create correlation maps, which are images that show where the actin and microtubule images are highly correlation (white) or anti-correlations (black). We created these maps by sweeping a square window to selection the region over which we calculated the normalized cross correlation. The interrogation window, defined by characteristic size d, contained $(2d + 1)^2$ pixels. Correlation maps could be created using different window sizes, calculating the normalized cross correlation (Eq. 1) over the $n = (2d + 1)^2$ pixels, and assigning the central pixel of the window with the correlation value. The borders of the correlation map were trimmed by removing d pixels from the borders as this method leaves a frame of uncalculated pixel values [59].

We used different interrogation window sizes to calculate correlation maps and determine the optimal window size, *d,* based on the diffraction limitation of optical microscopy and the quality of the resulting image. In order to compare between experiments, we averaged the correlation values from the entire correlation map to give a single number for the normalized cross correlation of one set of actin and microtubule images.

Results and Discussion

To assess the dynamics of the composite network of actin and microtubule filaments, we co-polymerized actin filaments and microtubules so as to have similar total polymer length and mesh sizes. We systematically altered the actin crosslinkers:actin monomers ratio, *R,* and the percentage of tubulin dimers bound to MAP65 crosslinkers (%). These control parameters resulted in altered arrangements of the network structure and tuned the mobility of the networks.

Composite network without actin crosslinkers

We first looked at the mobility of a composite network of actin and microtubule filaments with no actin crosslinkers present. To crosslink microtubule filaments, we tested MAP65 at 0%, 3%, and 10%, and recorded fluorescence images of the actin and microtubules (Fig. 1A). At 0% MAP65, the composite network of actin and microtubules co-polymerized to form an entangled network, as we have previously examined [13,14]. The microtubule filaments and tracer actin filaments showed little structure when imaged in wide field epi-fluorescence (Fig. 1A, i-iii). When MAP65 was introduced to the system (3%), microtubule filaments formed thin, over 10 μm long, bundles (Fig. 1A, iv-vi). The bright background in the microtubule channel suggests the presence of microtubules that remained un-crosslinked. The actin filaments were uniformly distributed as well, implying that they are unaffected by the microtubule crosslinking at this concentration.

At 10% MAP65, the microtubule bundles were denser and longer (Fig. 1A, vii-ix). The background in the microtubule channel was lower, implying that most microtubules were in bundles. Unlike at the lower concentrations, MAP65 at 10% displayed actin structures. Interestingly, the actin bundles appear to be coincident with the microtubule structures. The co-localization of actin filaments and crosslinked microtubule filaments is obvious in the merged channel (Fig. 1A, ix).

In addition to the organization of the networks, we directly quantified the mobility of the composite networks, as we have previously measured [13,14]. The mobility was deduced from the average standard deviation normalized by the average intensity, $\langle\delta\rangle/\langle I\rangle$, from time series data of the microtubule and actin fluorescence channels, separately. These data were taken for several fields within a chamber to perform the averaging (N = 5 - 10 measured time series for each chamber). Interestingly, the mobility of composite

networks with zero actin crosslinking ($R = 0$) and increasing microtubule crosslinking by MAP65 at 0%, 3%, and 10% did not depend on the MAP65 crosslinking, despite the noticeable change to the structure of the composites (Fig. 1B).

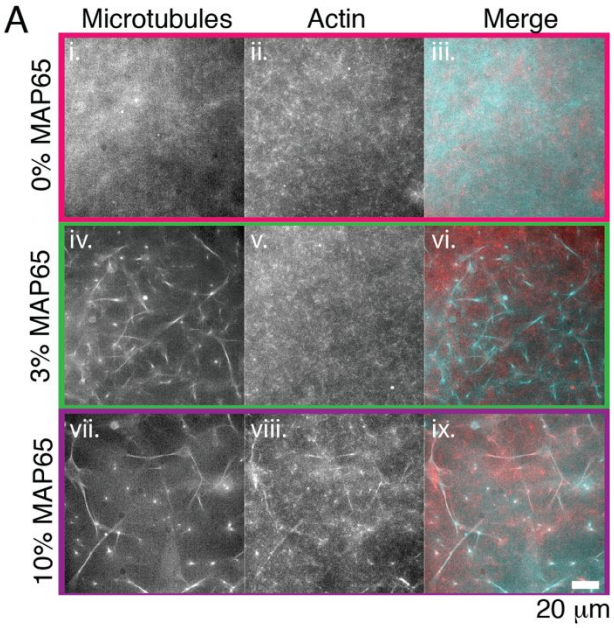

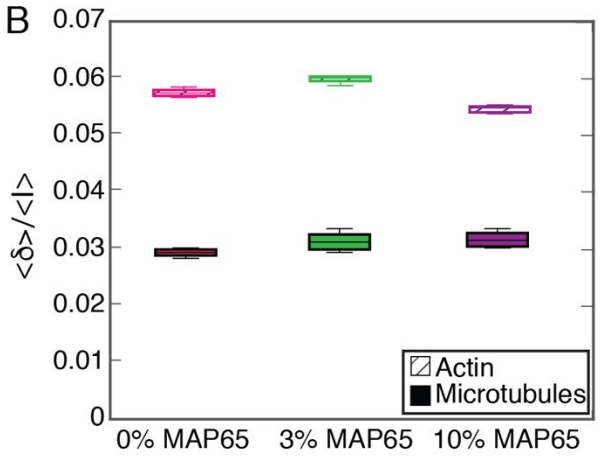

Figure 1. Composite networks of microtubule and actin filaments without actin crosslinkers. (A) Representative images of (i, iv, vii) microtubules, (ii, v, viii) actin filaments, and (iii, vi, ix) merge channels with microtubules (cyan) and actin (red) for 0%, 3%, and 10% MAP65 without actin crosslinking ($R = 0$). Colors outlined correspond to the colors in part (B). Scale bar is 20 μm. **(B)** The standard deviation of pixel intensity over time and space, $\langle\delta\rangle$, was calculated and normalized by the average of pixel intensity over time and space, $\langle I\rangle$. Box-whisker plot for $\langle\delta\rangle/\langle I\rangle$ ratio for 0%, 3%, and 10% MAP65 (N = 7, 8, 6 independent time series) is shown separately for actin (hashed) and microtubule (solid) networks.

Co-localization of microtubule and actin

We were surprised to observe that actin and microtubules co-localized at high MAP65 (10%). Although the co-localization appeared obvious, we sought to quantify the amount of co-localization using a cross-correlation between the actin and microtubule signals in the same location (Fig. 2, Supp. Fig. S1). Each image was 2048x2048 pixels with a magnified pixel size of 108 nm; the cross-correlation value for each pixel exists between +1 to -1. The brightest white points corresponded to highly correlated areas with the magnitude of +1; the darkest black regions indicate anticorrelation between the images with a value of -1. Cross correlations between actin and microtubule channels were calculated using different interrogation window sizes, *d*, where *d* is the number of pixels in both directions around the central pixel (Fig. 2B).

We found that the interrogation window size did impact our analysis. If the window size was too small ($d = 1$), the data was dominated by shot noise, which is uncorrelated, by definition (Fig. 2Bi). Considering the diffraction limit for these images was 250 – 325 nm or ~3 pixels, any calculation for window size below that does not carry physical information and would be dominated by noise, as shown for the smallest window size. When $d = 5$, there are bright patterns that correspond to the co-localized actin and microtubule bundles, indicating that actin and microtubule channels are highly correlated at those locations (Fig. 2Bii). These bright areas expand at window sizes of 10 and 15 pixels (Fig. 2Biii-iv). However, when the window size increased, the resolution of the structure decreased. The signal from the bundle was smeared out over the window, and information was lost. Due to this empirical assessment, we chose a window size of $d = 5$ to perform all cross-correlation analysis to quantify and compare the actin-microtubule co-localization.

We assessed that the cross correlation was not a result of fluorescence bleed-through between the actin and microtubule channels. This is obvious from inspection of several images where highly fluorescent, non-bundled regions in the microtubule channel are not bright in the actin channel (Fig. 2A, arrows, Supp. Fig. S2). These variations in microtubule intensity are likely clumps of aggregated tubulin protein that are incapable of forming filaments. Our tubulin clarification procedure removes most of these aggregates, but some always remain. In this case, the aggregates were useful to demonstrate that the co-localization we observe was not due to signal bleed through.

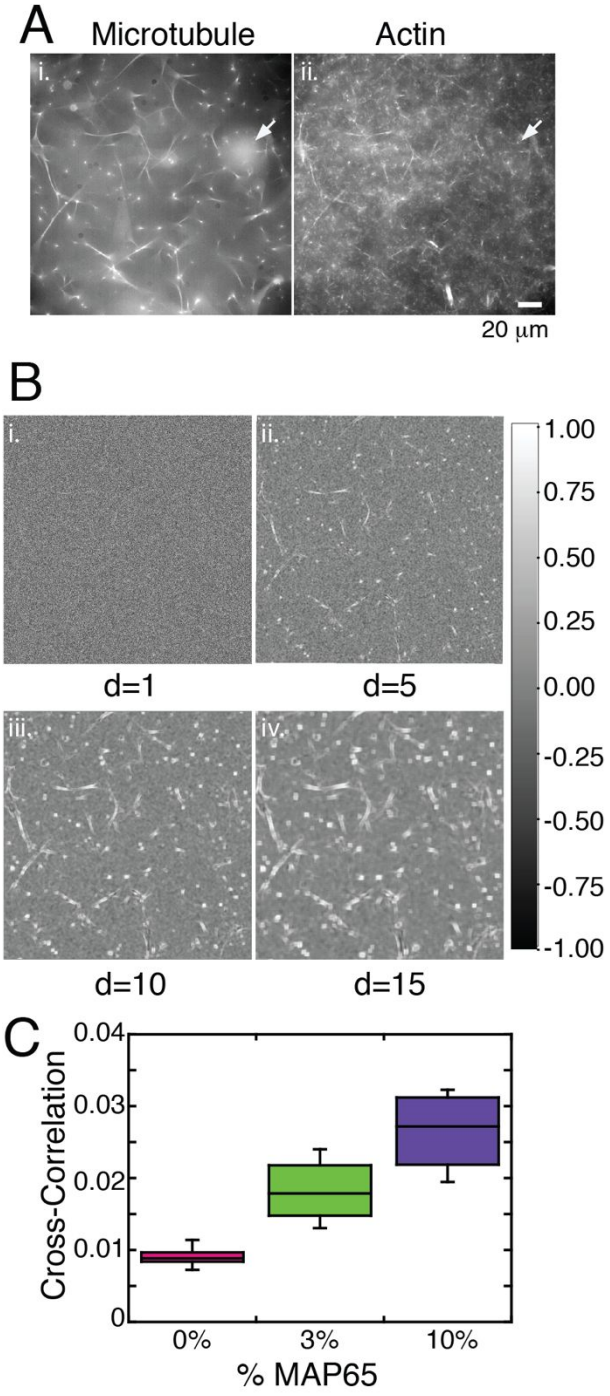

Figure 2. Cross correlation of microtubule and actin channels. (A) Representative image of (i) microtubule and (ii) actin networks in the same location for $R = 0$ and 10% MAP65. Scale bar is 20 μm. Bright regions in the microtubule channel (arrow) are not observed in the actin channel, implying bleed-through is not present. **(B)** Calculated cross-correlation maps for the same microtubule and actin images from (A) for different window sizes, d, when $d = 1$, 5, 10, 15 (i-vi). Optimal window size was chosen to be $d = 5$ ($n = 121$ pixels) and used throughout to compare different experiments. **(C)** Box-whisker plots of the average cross correlations between microtubule and actin channels averaged over the entire cross-correlation map created with window size $d = 5$ pixels for networks with no actin crosslinking ($R = 0$) and increasing MAP65 0%, 3%, 10%. (N = 8, 9, 8 independent time series)

Using the optimal window sizes, we can compare the cross correlation of the actin and microtubule signals as a function of MAP65 concentration. In the absence of actin crosslinkers, the cross correlation was an accurate reporter of what was obvious from images: the actin co-localization increased with MAP65 percent bound (Fig. 2C). Given the dependence on MAP65 concentration, we can think of two possible mechanisms for this co-localization: (1) actin can bind to MAP65 with a low affinity and is being co-crosslinked into bundles with microtubules, or (2) microtubule bundles are sweeping up the actin into the large bundles of microtubules. In order to assess these two possible mechanisms, we performed control experiments to examine the organization of actin in the presence of MAP65 without microtubules present. We found that in the presence of 10% MAP65, actin appeared as typical entangled networks with no effect on the actin structure (Fig. 3A). In order to be sure that the MAP65 was not associating with actin filaments – even weakly – we repeated the measurement using a GFP-labeled MAP65 and imaged the network in both channels (Fig. 3B). We found no obvious association of the MAP65 with actin and no structure in the MAP65 channel to imply interaction between the filaments (Fig. 3B).

Finally, by closely examining regions where we did observe co-localization between microtubules and actin, we found that particularly thick microtubule bundles in the presence of 10% MAP65 could show individual actin filaments within larger bundle structures (Fig. 3C). We used ImageJ/FIJI to create a temporal color code of the time series for the actin and microtubule channels, which overlaid successive images in different colors, as given by the time-color scale (Fig. 3D). When using a spectrum color scale, parts of the image that did not move over time appear white (all colors) in the temporal color code image. The microtubule bundle was mostly white due to low fluctuations (Fig. 3Di). Most of the actin filaments appeared as rainbows because they were able to fluctuate (Fig. 3Dii). The actin filaments that were co-localized with the microtubule bundle displayed as white – implying that they did not fluctuate over time, likely because they were stuck inside the microtubule bundle. Prior work has shown that the spacing between microtubules within MAP65 driven bundles is 25 – 35 nm [60] , more than enough space to trap an actin filament of width of 10 nm. Together, these observations support a mechanism where the actin is swept up into the microtubule bundles and not being co-crosslinked with microtubules due to an interaction between MAP65 and actin.

The mechanism for actin-microtubule co-localization mediated by MAP65 is different from previously reported actin-microtubule interactions mediated by proteins originally thought to be only actin or microtubule binding partners. In those prior reports, naturally occurring proteins, such as CLIP-170, mDia [61], or engineered proteins, such as TipAct [48] served as crosslinkers between individual growing actin or microtubules and surprisingly altered the growth rates as well as the organization of these filaments. Another exciting study used tau and fascin to co-organize actin and microtubules [52]. In all of these examples, the experiments showed specific interactions between the filaments and the crosslinkers. Further, these experiments were performed in quasi-2D, which is distinct from the work presented here, which is specifically interested in 3D networks of actin-microtubule composites. Ultimately, these exciting co-crosslinkers can be utilized to alter the properties of the 3D networks we are creating in this paper.

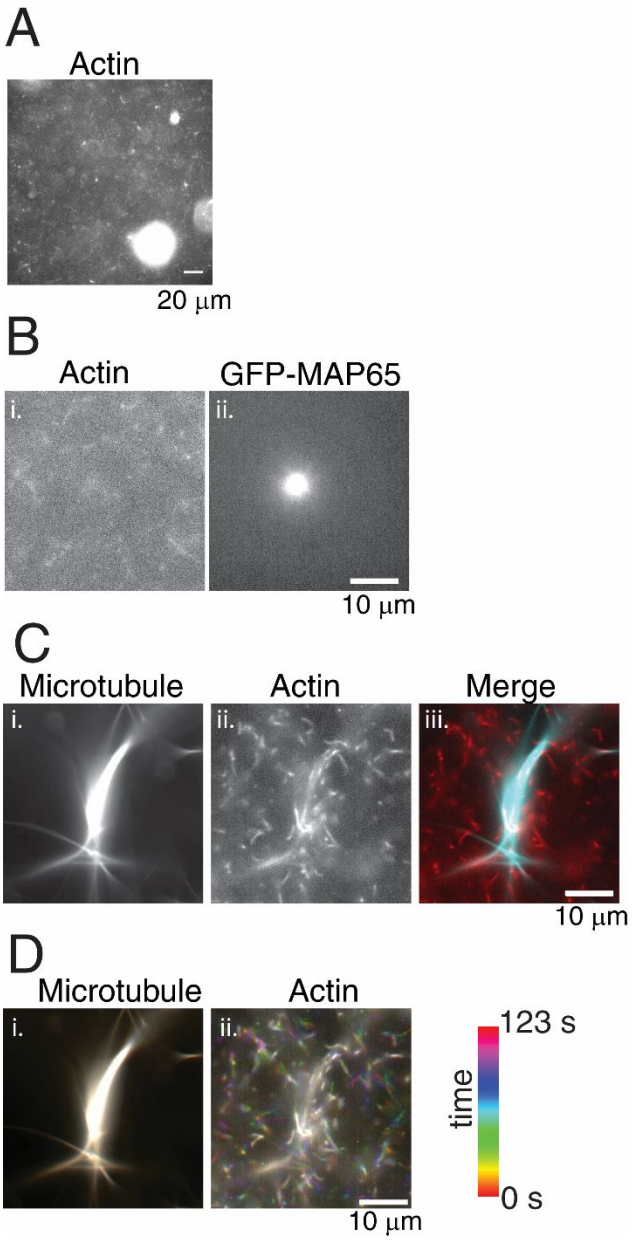

Figure 3. Actin and MAP65 do not interact without microtubules. (A) Actin network with 10% MAP65. Scale bar is 20 μm. **(B)** Representative image of (i) actin and (ii) GFP-MAP65. Scale bar is 10 μm. **(C)** (i) Large, thick bundle of microtubules in the presence of 10% MAP65. (ii) Actin filaments co-localized within the bundle. (iii) Merge of microtubules (cyan) and actin (red). Scale bar is 10 μm. **(D)** Temporal color code of a 1-minute time series of (i) microtubules and (ii) actin shows that actin within the microtubule bundle does not fluctuate as much as actin outside of the bundles. Temporal color code scale uses the spectrum color scale from 0 – 123 s.

The role of actin crosslinkers in the fluctuation dynamics of actin and microtubules

We have previously shown that actin network crosslinking has a profound effect on the mobility and viscoelastic nature of actin-microtubule composite networks [13,14]. In our prior works, the microtubule network was less dense compared to the actin network, which may have been the reason for the actin's control over the mechanical properties. To determine the impact of actin crosslinking by NeutrAvidin when actin and microtubule mesh sizes are comparable, we prepared co-polymerized actin and microtubule filaments without MAP65 crosslinkers, and with an increasing ratio of NeutrAvidin:actin R = 0, 0.02, 0.04, and 0.08. The actin and microtubule networks were imaged directly and the organization and mobility were measured for each filament type using time series.

We found that the microtubule network of the composite did not appear to have gross changes in morphology as the actin crosslinking ratio was increased (Fig. 4A). Actin filaments did tend to form a mesh-like network with some clusters of filaments at the highest tested ratio, R = 0.08, similar to our prior results [13]. NeutrAvidin molecules have four potential binding sites in a tetrahedral arrangement allowing the actin network to be oriented in a variety of angles when crosslinked. While some actin bundling can occur, the actin bundles are far less obvious than the microtubule bundles created by the antiparallel crosslinker, MAP65.

For multiple locations in several chambers, the mobility $<\delta>/<I>$ was measured and compared for networks without microtubule crosslinking and increasing actin crosslinking (R = 0, 0.02, 0.04, 0.08). In general, we found that the mobility of both actin and microtubules depended on the actin crosslinking (Fig. 4B). This indicated that the network mobility and viscoelastic properties were controlled by the actin network and its crosslinking ratio [13].

Of interest, we found that the microtubule mobility increased, while the actin mobility decreased (Fig. 4B). Perhaps it is not surprising that actin would become less mobile when crosslinked. Indeed, we have shown that in our prior work [18,19,49]. Strikingly, and distinct from our prior work, microtubule motility significantly increased as the actin crosslinking increased. The enhanced microtubule mobility may result from the increased free space when actin filaments become crosslinked, giving microtubules more space to fluctuate. This implied that the actin was bundling on a scale that was smaller than we can detect in the microscope, as we previously noted [18,19,49].

In our prior works, the actin mobility is almost always higher than the microtubule mobility due to the inherent high flexibility of actin filaments compared to microtubule filaments [18,19,49]. These prior works often had equimolar actin monomers and tubulin dimers, resulting in more actin filaments than microtubules. Specifically, the number of actin filaments was greater than the number of microtubules due to the fact that the microtubule requires 13 dimers to nucleate and form a filament, compared to two actin monomers needed for actin filaments. Here, we purposely chose an actin-microtubule ratio to result in similar amounts of actin and microtubule polymer length and mesh sizes. In this study, the tubulin fraction is ~87%. In one prior work, we altered the relative ratio of actin and tubulin to change the network from 100% actin to 100% microtubules for entangled networks without crosslinkers. Significant changes in the mobility and mechanics of the network occurred when the actin and microtubule polymer mass were similar [49]. In that study, entangled networks with high fractions of tubulin had low mobilities for actin and microtubules, with actin's mobility slightly higher than microtubules [49]. Excitingly, we show here that when actin-microtubule filament ratios are more similar, the mobility of actin decreases as a function of actin crosslinking, and the microtubule mobility increases.

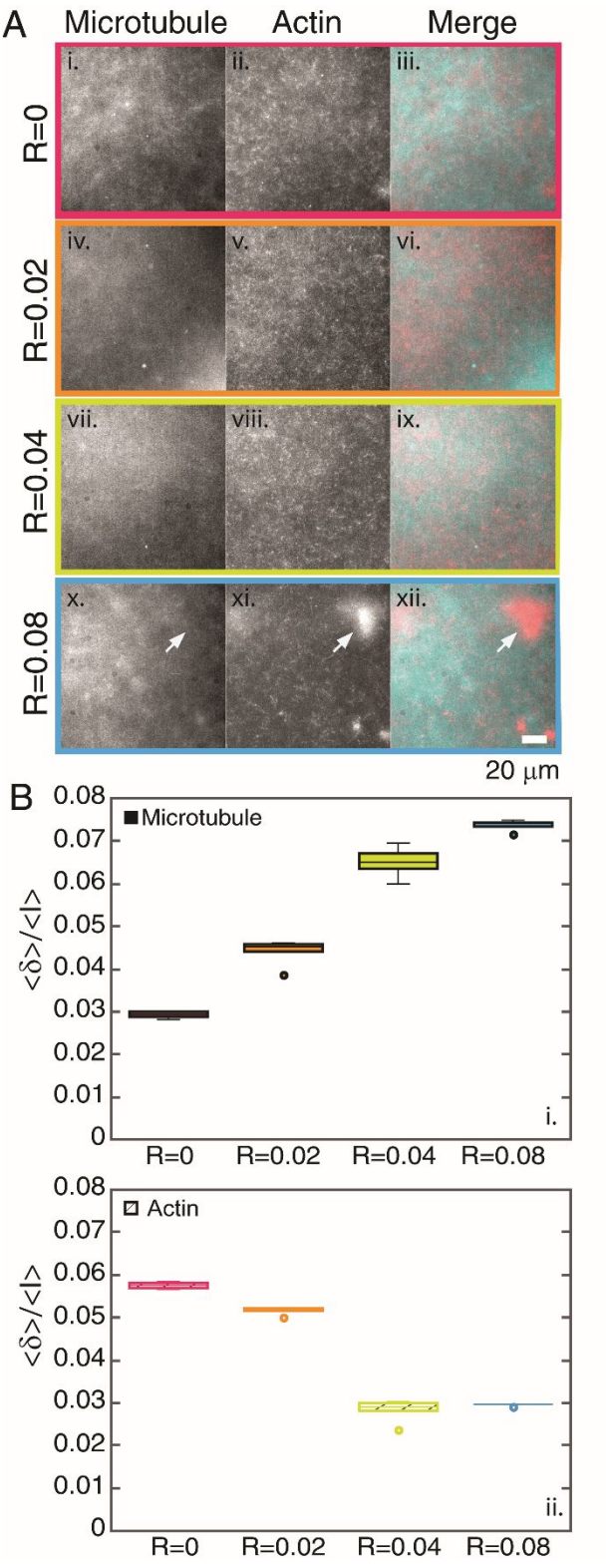

Figure 4. Filament fluctuations depend on actin crosslinking. (A) Representative images of microtubules (i, iv, vii, x) and actin (ii, v, viii, xi). Merged images (iii, vi, ix, xii) display microtubules (cyan) and actin (red) networks as the actin crosslinking is increased R = 0, 0.02, 0.04, 0.08 in the absence of microtubule crosslinkers (N = 7, 6, 8, 5 independent time series for increasing R). Colors outlined correspond to the colors in part (B). Scale bar is 20 μm. Arrows denote regions where there is high fluorescence in one channel without bleed-through into the other fluorescence channel. **(B)** The mobility of the networks was quantified using the $\langle\delta\rangle/\langle I\rangle$ ratio where $\langle\delta\rangle$ is the standard deviation of pixel intensity that was averaged over time and space and then normalized by the mean of pixel intensity, $\langle I\rangle$, for (i) microtubules and (ii) actin as a function of actin crosslinking ratio.

High microtubule crosslinking causes co-localization of actin and microtubules, while actin crosslinking controls filament mobility

We previously discussed the co-localization of actin and microtubule filaments in the absence of actin crosslinkers ($R = 0$) and demonstrated that it was highly correlated at 10% MAP65 (Figs. 1,2). We wanted to test if the actin crosslinking had further effects to enhance or negate the actin-microtubule co-localization driven by MAP65. To investigate this phenomenon, we changed the NeutrAvidin:actin ratio, (R) systematically while maintaining the MAP65 at 10% bound (Fig. 5). For all actin crosslinker ratios ($R = 0$, 0.02, 0.04, 0.08), the microtubules displayed long bundles distributed randomly through the whole sample in the imaging plane as well as the depth of the experimental chamber (Fig. 5A). As for the entangled networks, actin filaments appeared to co-localize with the microtubule bundles (Fig. 5A).

We quantified the co-localization using cross-correlation maps with the optimal window size of $d = 5$ (Fig. 5B). All the networks had high cross correlation between actin and microtubules when high MAP65 (10%) was present, and there was no significant change in the cross correlation due to the actin crosslinking ratio (Fig. 5B).

We measured the mobility of actin and microtubules in composite networks with high microtubule crosslinking (MAP65 at 10%) as a function of actin crosslinking ratio (R). As above, we determined the mobility of this crosslinked network by measuring the mean of standard deviation over time, $<\delta>$, and the mean of intensity over time, $<I>$, when the actin crosslinking was $R = 0$, 0.02, 0.04, and 0.08. For microtubules, the mobility increased as more actin crosslinkers were added (Fig. 4C). For actin filaments, adding more actin crosslinkers reduced actin filament mobility. The trend for both actin and microtubules was similar for 10% MAP65 as shown above for 0% MAP65 (Fig. 3B). These results imply that the actin crosslinkers have the most influence on network mobility. From our prior work with actin-microtubule composites, we also know that the viscoelastic properties of the networks depend on the actin network mobility, implying that the MAP65 has little effect on the network mechanics.

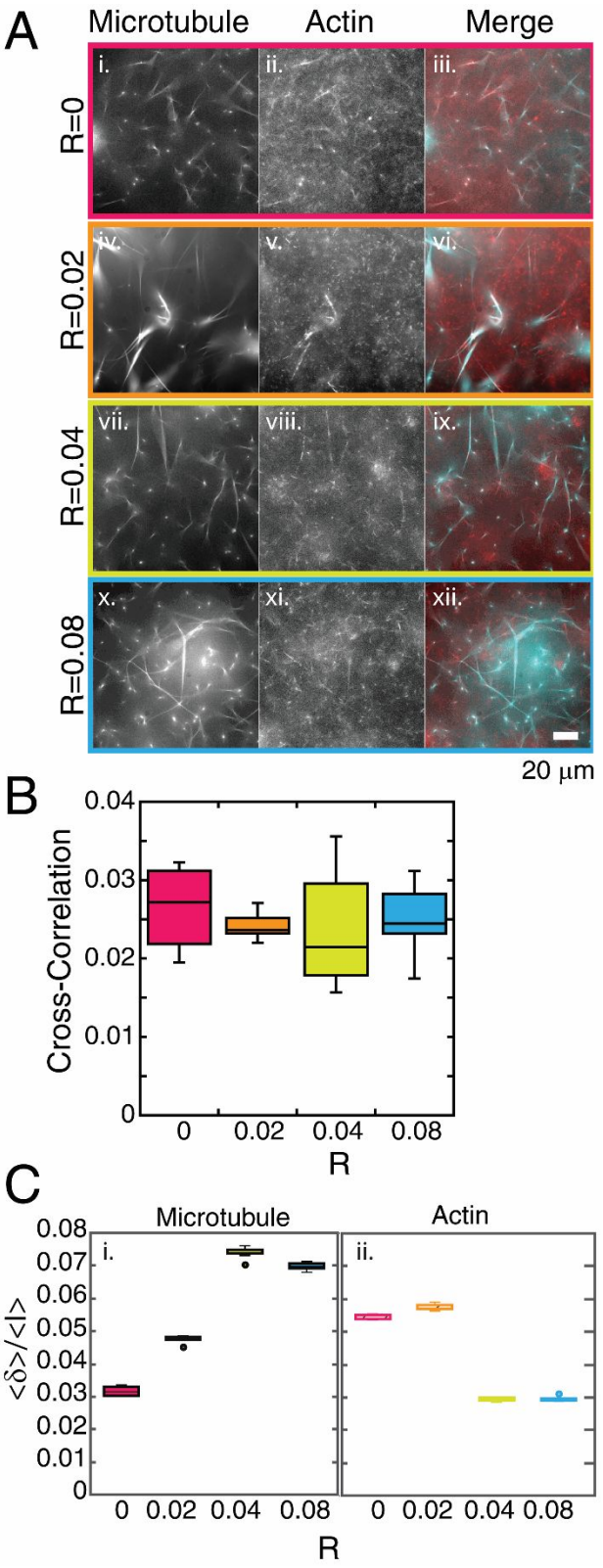

Figure 5. Co-localization of microtubule and actin filaments at 10% MAP65. (A) Representative images of microtubules (i, iv, vii, x), actin (ii, v, viii, xi), and merge (iii, vi, ix, xii) with microtubules (cyan) and actin (red) composite networks created in the presence of 10% MAP65 with different actin crosslinking ratios: R = 0, 0.02, 0.04, and 0.08. Bundles of microtubules and co-localization of actin are obvious for all networks. Color outlines correspond to the data represented in (B) and (C). Scale bar is 20 μm. **(B)** Cross correlation of microtubule and actin channels were computed and displayed in a box-whisker plot. There was no significant difference in the actin-microtubule co-localization as a function of R (N =8, 8, 10, 10). **(C)** The mobility of the (i) microtubules and (ii) actin of composite networks was quantified using the $\langle\delta\rangle/\langle I\rangle$ ratio where $\langle\delta\rangle$ is the standard deviation of pixel intensity that was averaged over time and space and then normalized by the mean of pixel intensity, $\langle I\rangle$, for networks with increasing actin crosslinkers, R (N = 6, 6, 8, 9 independent time series).

We showed that microtubule bundling by MAP65 can significantly affect the organization of actin and microtubules, specifically causing co-localization (Figs. 1,2,5). Using the GFP-labeled MAP65 protein, we can perform three-color imaging to localize the microtubules, actin, and MAP65 simultaneously (Fig. 6A). For an example network with 10% MAP65 and $R = 0.02$ actin crosslinking, we found that the MAP65 and microtubules exactly correlated their organizations. The actin also correlated with the microtubules and MAP65, but there were additional actin filament signals outside of the bundles (Fig 6Aii). Using the temporal color code, it is clear that the actin associated with the bundles is not as mobile as the actin in the background, also shown in figure 3 (Fig. 6B, 3D).

Although the microtubule crosslinker had profound effects on the microtubule and actin organizations, it had insignificant effects on the mobility of the actin and microtubule filaments (Fig. 6C). This trend continued for all variations of Netravidin crosslinker (R = 0, 0.02, 0.04, 0.08) and MAP65 percentage bound (0%, 3%, 10%) (Fig. 6C). One interesting future avenue would be to explore other microtubule bundling agents. It is known that MAP65 crosslinkers reduce the flexural rigidity of microtubule filaments [62], but other microtubule-associated proteins, such as tau, make microtubules stiffer [7,63]. Future studies using these crosslinking and stiffening associated proteins could have different results on the mobility.

In order to ensure that these effects on mobility were not caused by inadvertent effects of the crosslinkers to the wrong filament within the network, we performed control experiments with actin in the presence of MAP65 (Fig. 3) and microtubules in the presence of Neutravidin (Supp. Fig. S3). For each of these tests, we used the higher crosslinker concentration (10% MAP65 and R = 0.08). The mobility of these networks were measured and shown as a gray bar (Fig. 6C). For microtubules in the presence of NeutrAvidin, the median mobility is similar to that of microtubules with $R = 0$ (Fig. 6C i-iv), implying that the control network behaves like the composite without actin crosslinkers (Fig. 6). Consequently, we can conclude that microtubule filaments and NeurAvidin molecules do not interact in this composite network. Further, the higher mobility than control could be due to the increased volume compared to when the other part of the network is present.

For the samples with actin in the presence of MAP65, without microtubules and without NeutrAvidin (R = 0), the median and the distribution of mobility exhibited higher mobility compared to 10% MAP and $R = 0$ in the presence of microtubule filaments. This result mirrors the imaging results (Fig. 3) that suggest that MAP65 and actin do not associate to form bundles of actin. implies that great amount of MAP65 could not form bundles of actin filaments and did not lower the mobility of actin network as was shown for higher R values. Interestingly, the mobility of the actin in the absence of microtubules was significantly higher than observed with microtubules present (Fig. 6C v-viii). This could be due to the increased volume to move when the microtubules were absent.

One interesting observation was that, despite the co-localization of actin with microtubules when the MAP65 was 10% (Fig. 2,4), the actin mobility is not equal to the microtubule mobility. This result implied that these co-localized actin filaments did not dominate the fluctuation dynamics in the actin network. That is corroborated by the imaging data and the temporal color code data of the actin which shows significant mobility from the free actin filaments, despite a fraction being immobilized in the bundles (Fig. 3D, 6B).

We also noted that there was a relatively large jump in actin mobility when doubling the actin crosslinker concentration from $R = 0.02$ to 0.04. An additional doubling of the actin crosslinkers ($R = 0.08$) has no further effect, as if the network mobility has hit a saturation level (Fig. 6). This same activity was observed in our recent publication examining actin crosslinking in composite networks [14].

Unlike actin, the microtubules did not show a discrete jump in the mobility as a function of actin crosslinking. Instead, the trend of increasing microtubule mobility was gradual as a function of actin crosslinking (Fig. 5). Comparing this data to our recent publication of actin crosslinking in composites without microtubule crosslinking, we see similar results [14]. Namely, the microtubule mobility appears higher than the actin mobility for $R = 0.04$-0.08. We conjecture that the mobility changes come from actin

bundles at a level that allows increased microtubule mobility, but is too small to observe with the resolution of the light microscope.

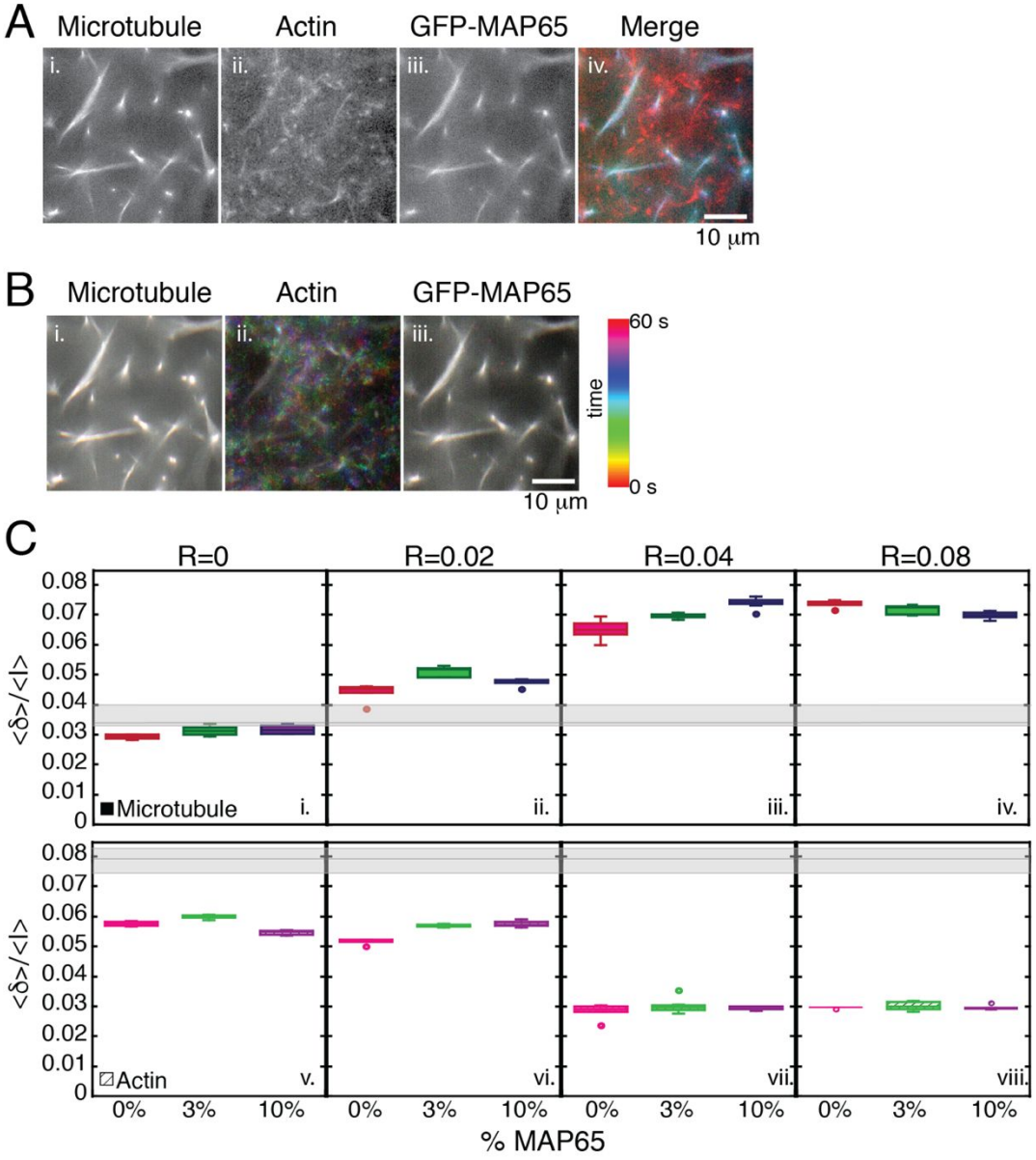

Figure 6. Mobility of composite networks of microtubule and actin filaments with varying crosslinkers. (A) Example three-color image of a network with (i) microtubules and (ii) actin crosslinked with (iii) 10% GFP-MAP65, and NeutrAvidin R = 0.02. Three-color image merge showing microtubules (blue), MAP65 (green), and actin (red). Scale bar is 10 μm. **(B)** Example mobility of the images from (A) using ImageJ/FIJI temporal color code function shows (i) microtubules, (ii) actin, and (iii) MAP65. Microtubules and act both do not move, which a subset of actin does move outside of the bundles. **(C)** All mobility measurements for microtubules (i – iv) and actin (v- viii) as a function of actin crosslinking (R) and MAP65 binding show an overall dependence on actin crosslinking but not on MAP65 binding (N = 5 - 10 independent time series). Horizontal gray bars denote control data of only one type of filament in the network.

Discussion and Conclusions

Composite actin and microtubule networks are important regulators of intracellular organization and mechanics. We found here that the microtubule crosslinking and bundling can control the organization of actin-microtubule networks, but the actin crosslinking controls the dynamics of both filament types, and likely the mechanics of the network. This result was rather unexpected given that one of the tenants of biological and soft matter is a relationship between structure and function. In this composite network, the obvious morphological changes driven by microtubule crosslinking by MAP65 (ie. the large co-localized actin-microtubule bundles), are not affecting the dynamics nor the mechanics of the entire network, as might have been predicted.

Despite the large structural changes, the fluctuation dynamics of the composite network are controlled only by the actin portion, and the extent of crosslinking of the actin. Reorganization of the network due to actin crosslinking is difficult to distinguish given the resolution of fluorescence microscopy, but we expect that the actin filaments are locally bundled and linked. Despite the lack of obvious change of the organization with actin crosslinking, the fluctuations of the actin and microtubules change significantly. Of particular interest is that the microtubules become the more mobile fraction of the network when the actin filaments are highly crosslinked ($R > 0.02$). We observed this effect in a recent publication when $R = 0.04 – 0.08$, but the apparent change in mobility and the difference between actin and microtubule mobilities were not as striking in that prior study as we present here (Fig. 5). The difference could be due to the increased number of microtubule filaments compared to our prior work or the higher labeling of the microtubules revealing a more mobile population. Future work with active crosslinkers (motors) of either actin or microtubules could reveal exciting mechanical feedback when included in composite cytoskeletal networks with stable crosslinkers.

Acknowledgements

This research was funded by William M. Keck Foundation Research Grant (awarded to R.M.R.-A., J.L.R., M.D., and M.J.R.). L. Farhadi was partially supported by NSF MRSEC DMR-1420382 to Seth Fraden.

References

1 P. A. Janmey, S. Hvidt, J. Kasso, D. Lerchess, A. Maggsoo, E. Sackmannllii, M. Schliwa and T. P. Stosselson, *J. Biol. Chem.*, 1994, **269**, 32503–32513.

2 F. Huber, A. Boire, M. P. López and G. H. Koenderink, *Curr. Opin. Cell Biol.*, 2015, **32**, 39–47.

3 Q. Wen and P. A. Janmey, *Curr Opin Solid State Mater Sci*, 2012, **15**, 177–182.

4 K. Rottner and M. Schaks, *Curr. Opin. Cell Biol.*, 2019, **56**, 53–63.

5 F. Gittes, B. Mickey, J. Nettleton and J. Howard, *J. Cell Biol.*, 1993, **120**, 923–934.

6 M. S. Yasar, D. Sept, J. Li, T. L. Hawkins, J. L. Ross, M. Mirigian and D. L. Sackett, *Cell. Mol. Bioeng.*, 2012, **5**, 227–238.

7 T. L. Hawkins, D. Sept, B. Mogessie, A. Straube and J. L. Ross, *Biophys. J.*, 2013, **104**, 1517–1528.

8 K. A. Ganzinger and P. Schwille, *J. Cell Sci.*, 2019, **132**, jcs227488.

9 Y. Bashirzadeh and A. P. Liu, *Soft Matter*, 2019, **15**, 8425–8436.

10 D. Hürtgen, S. K. Vogel and P. Schwille, *Adv. Biosyst.*, 2019, **3**, 1–11.

11 H. Hess and J. L. Ross, *Chem. Soc. Rev.*, 2017, **46**, 5570–5587.

12 D. Needleman and Z. Dogic, *Nat. Rev. Mater.*, 2017, **2**, 17048.

13 S. N. Ricketts, M. L. Francis, L. Farhadi, M. J. Rust, M. Das, J. L. Ross and R. M. Robertson-Anderson, *Sci. Rep.*, 2019, **9**, 1–12.

14 M. L. Francis, S. N. Ricketts, L. Farhadi, M. J. Rust, M. Das, L. Ross and R. M. Robertson-anderson, *Soft Matter*, 2019, **15**, 9056–9065.

15 A. C. H. Murphy and P. W. Young, *Cell Biosci.*, 2015, **5**, 1–9.

16 P. A. Janmey, *Proc. Natl. Acad. Sci. U. S. A.*, 2001, **98**, 14745–14747.

17 B. Grooman, I. Fujiwara, C. Otey and A. Upadhyaya, *PLoS One*, 2012, **7**, e42773.

18 O. Lieleg, M. M. A. E. Claessens, C. Heussinger, E. Frey and A. R. Bausch, *Phys. Rev. Lett.*, 2007, **99**, 1–5.

19 A. Bretscher, *Proc. Natl. Acad. Sci. U. S. A.*, 1981, **78**, 6849–6853.

20 D. S. Courson and R. S. Rock, *J. Biol. Chem.*, 2010, **285**, 26350–26357.

21 D. H. Wachsstock, W. H. Schwarz and T. D. Pollard, *Biophys. J.*, 1994, **66**, 801–809.

22 D. S. Seara, V. Yadav, I. Linsmeier, A. P. Tabatabai, P. W. Oakes, S. M. A. Tabei, S. Banerjee and M. P. Murrell, *Nat. Commun.*, 2018, **9**, 1–10.

23 C. P. Broedersz, M. Depken, N. Y. Yao, M. R. Pollak, D. A. Weitz and F. C. MacKintosh, *Phys. Rev. Lett.*, 2010, **105**, 238101.

24 Y. Tseng, B. W. Schafer, S. C. Almo and D. Wirtz, *J. Biol. Chem.*, 2002, **277**, 25609–25616.

25 B. Edozie, S. Sahu, M. Pitta, A. Englert, C. F. Do Rosario and J. L. Ross, *Soft Matter*, 2019, **15**, 4797–4807.

26 M. Dogterom and T. Surrey, *Curr. Opin. Cell Biol.*, 2013, **25**, 23–29.

27 J. Roostalu, J. Rickman and C. Thomas, *Cell*, 2018, **175**, 796-808.e14.

28 M. P. N. Juniper, M. Weiss, I. Platzman, J. P. Spatz and T. Surrey, *Soft Matter*, 2018, **14**, 901–909.

29 M. Vleugel, S. Roth, C. F. Groenendijk and M. Dogterom, 2016, **114**, 54278.

30 D. Needleman and Z. Dogic, *Nat. Rev. Mater.*, 2017, **2**, 17048.

31 S. J. DeCamp, G. S. Redner, A. Baskaran, M. F. Hagan and Z. Dogic, *Nat. Mater.*, 2015, **14**, 1110–1115.

32 S. Wijeratne and R. Subramanian, *Elife*, 2018, **7**, 1–28.

33 J. Gaillard, E. Neumann, D. Van Damme, V. Stoppin-Mellet, C. Ebel, E. Barbier, D. Geelen and M. Vantard, *Mol. Biol. Cell*, 2008, **19**, 4534–4544.

34 M. Braun, Z. Lansky, G. Fink, F. Ruhnow, S. Diez and M. E. Janson, *Nat. Cell Biol.*, 2011, **13**, 1259–1264.

35 Z. Lansky, M. Braun, A. Lüdecke, M. Schlierf, P. R. Ten Wolde, M. E. Janson and S. Diez, *Cell*, 2015, **160**, 1159–1168.

36 K. T. Stanhope, V. Yadav, C. D. Santangelo and J. L. Ross, *Soft Matter*, 2017, **13**, 4268–4277.

37 G. Henkin, S. J. DeCamp, D. T. N. Chen, T. Sanchez and Z. Dogic, *Philos. Trans. R. Soc. A Math. Phys. Eng. Sci.*, 2014, **372**, 20140142–20140142.

38 M. Bai, W. S. Klug, M. T. Valentine, A. J. Levine and Y. Yang, *Soft Matter*, 2012, **9**, 383–393.

39 Y. C. Lin, G. H. Koenderink, F. C. MacKintosh and D. A. Weitz, *Macromolecules*, 2007, **40**, 7714–7720.

40 B. J. Lopez and M. T. Valentine, *Biochim. Biophys. Acta - Mol. Cell Res.*, 2015, **1853**, 3015–3024.

41 L. Farhadi, C. Fermino Do Rosario, E. P. Debold, A. Baskaran and J. L. Ross, *Front. Phys.*, 2018, **6**, 1–16.

42 S. Z. Wu and M. Bezanilla, *J. Cell Biol.*, 2018, **217**, 3531–3544.

43 Y. Cabrales Fontela, H. Kadavath, J. Biernat, D. Riedel, E. Mandelkow and M. Zweckstetter, *Nat. Commun.*, 2017, **8**, 1–12.

44 M. Dogterom and G. H. Koenderink, *Nat. Rev. Mol. Cell Biol.*, 2019, **20**, 38–54.

45 M. P. López, F. Huber, I. Grigoriev, M. O. Steinmetz, A. Akhmanova, M. Dogterom and G. H. Koenderink, *Methods Enzymol.*, 2014, **540**, 301–320.

46 K. Regan, D. Wulstein, H. Rasmussen, R. McGorty and R. M. Robertson-Anderson, *Soft Matter*, 2019, **15**, 1200–1209.

47 Y. C. Lin, G. H. Koenderink, F. C. MacKintosh and D. A. Weitz, *Soft Matter*, 2011, **7**, 902–906.

48 M. P. López, F. Huber, I. Grigoriev, M. O. Steinmetz, A. Akhmanova, G. H. Koenderink and M. Dogterom, *Nat. Commun.*, 2014, **5**, 1–9.

49 S. N. Ricketts, J. L. Ross and R. M. Robertson-Anderson, *Biophys. J.*, 2018, **115**, 1055–1067.

50 A. N. Ketene, E. M. Schmelz, P. C. Roberts and M. Agah, *Nanomedicine Nanotechnology, Biol. Med.*, 2012, **8**, 93–102.

51 Y. Tseng, T. P. Kole, J. S. H. Lee, E. Fedorov, S. C. Almo, B. W. Schafer and D. Wirtz, *Biochem. Biophys. Res. Commun.*, 2005, **334**, 183–192.

52 A. Elie, E. Prezel, C. Guérin, E. Denarier, S. Ramirez-, L. Serre, A. Andrieux, A. Fourest-lieuvin, L. Blanchoin and I. Arnal, *Sci. Rep.*, 2015, **5**, 9964.

53 V. Pelletier, N. Gal, P. Fournier and M. L. Kilfoil, *Phys. Rev. Lett.*, 2009, **102**, 100–103.

54 A. Tulin, S. Mcclerklin, Y. Huang and R. Dixit, *Biophysj*, 2012, **102**, 802–809.

55 J. Pringle, A. Muthukumar, A. Tan, L. Crankshaw, L. Conway and J. L. Ross, *J. Phys. Condens. Matter*, 2013, **25**, 374103.

56 M. L. Gardel, M. T. Valentine, J. C. Crocker, A. R. Bausch and D. A. Weitz, *Phys. Rev. Lett.*, 2003, **91**, 8–11.

57 Y. C. Lin, G. H. Koenderink, F. C. MacKintosh and D. A. Weitz, *Macromolecules*, 2007, **40**, 7714–7720.

58 G. M. Cooper, *The cell : a molecular approach*, Washington, D.C. : Sunderland, Mass. : ASM Press ; Sinauer Associates, 2nd ed., 2000.

59 Normalized cross-correlation sample code, https://dsp.stackexchange.com/questions/28322/python-normalized-cross-correlation-to-measure-similarites-in-2-images.

60 J. Chan, C. G. Jensen, L. C. W. Jensen, M. Bush and C. W. Lloyd, *Proc. Natl. Acad. Sci. U. S. A.*, 1999, **96**, 14931–14936.

61 B. L. G. Jessica L. Henty-Ridilla, Aneliya Rankova, Julian A. Eskin, Katelyn Kenny, *Science.*, 2016, **352**, 1004–109.

62 D. Portran, M. Zoccoler, J. Stoppin-MelletGaillard, V. Stoppin-Mellet, E. Neumann, I. Arnal, J. L. Martiel and M. Vantard, *Mol. Biol. Cell*, 2013, **24**, 1964–1973.

63 H. Felgner, R. Frank, J. Biernat, E. M. Mandelkow, E. Mandelkow, B. Ludin, A. Matus and M. Schliwa, *J. Cell Biol.*, 1997, **138**, 1067–1075.